

Supporting Information for

Mutual promotion effect between aerosol particle liquid water and nitrate formation lead to severe nitrate-dominated particulate matter pollution and low visibility

5 Yu Wang^{1,2,a}, Ying Chen^{3,a}, Zhijun Wu^{1,4,5,*}, Dongjie Shang¹, Yuxuan Bian⁶, Zhuofei Du^{1,b}, Sebastian H. Schmitt^{4,7,c}, Rong Su^{1,d}, Georgios I. Gkatzelis^{4,7,e,f}, Patrick Schlag^{4,7,g}, Thorsten Hohaus^{4,7}, Aristeidis Voliotis², Keding Lu^{1,4,5}, Limin Zeng^{1,4}, Chunsheng Zhao⁸, Rami Alfarra^{2,9}, Gordon McFiggans², Alfred Wiedensohler¹⁰, Astrid Kiendler-Scharr^{4,7}, Yuanhang Zhang^{1,4,5}, Min Hu^{1,4,5}

10 ¹State Key Joint Laboratory of Environmental Simulation and Pollution Control, College of Environmental Sciences and Engineering, Peking University, Beijing 100871, China

²Centre for Atmospheric Science, School of Earth and Environmental Sciences, The University of Manchester, Manchester M13 9PL, UK

³Lancaster Environment Centre, Lancaster University, Lancaster, LA1 4YQ, UK

15 ⁴International Joint Laboratory for Regional Pollution Control, 52425 Jülich, Germany, and Beijing 100871, China

⁵Collaborative Innovation Center of Atmospheric Environment and Equipment Technology, Nanjing University of Information Science and Technology, Nanjing 210044, China

⁶State Key Laboratory of Severe Weather, Chinese Academy of Meteorological Sciences, Beijing, 100081, China

20 ⁷Institute for Energy and Climate Research, IEK-8: Troposphere, Forschungszentrum Jülich, 52425 Jülich, Germany

⁸Department of Atmospheric and Oceanic Sciences, School of Physics, Peking University, Beijing 100871, China

25 ⁹National Centre for Atmospheric Science, School of Earth and Environmental Sciences, The University of Manchester, Manchester, M13 9PL, UK

¹⁰Leibniz Institute for Tropospheric Research, 04318 Leipzig, Germany

^aThese authors contribute equally to this work

30 ^bNow at Center for Urban Transport Emission Research & State Environmental Protection Key Laboratory of Urban Ambient Air Particulate Matter Pollution Prevention and Control, College of Environmental Science and Engineering, Nankai University, Tianjin, 300071, China

^cNow at TSI GmbH, 52068 Aachen, Germany

^dNow at Guangdong Science and Technology Monitoring and Research Center, Guangzhou 510033, China

^eNow at NOAA Earth Systems Research Laboratory, Boulder, Colorado 80305, United States

35 ^fNow at Cooperative Institute for Research in Environmental Sciences, Boulder, Colorado 80309, United States

^gNow at Shimadzu Deutschland GmbH, 47269 Duisburg, Germany

Correspondence to: Zhijun Wu (zhijunwu@pku.edu.cn)

Contents of this file

40 **Text S1** Measurement and methods (including Figure S1 – S5)

Results Figure S6 – S9

Table S1

Figure S1. The time series of mass concentration of POA and SOA in non-refractory PM₁ from ME2

45 (left axis) and the fraction of SOA in total organic (right axis) during the period from 29 February to 5 March, 2016.

Figure S2. The exemplified size distribution of $dM/d\log D_p$ and the classification of re-arranged aerodynamic diameter size range.

Figure S3. Average size distribution of NH_4^+ , NO_3^- , SO_4^{2-} , Cl^- , Org (in stokes diameter), in the period of 50 February 29 to March 5, 2016.

Figure S4. Comparison of particle number size distribution from measurement and four-mode lognormal fitting method.

Figure S5. Comparison of sized-resolved κ from H-TDMA measurement and the calculated size distribution of κ from 3 nm to 10 μm .

55 **Figure S6.** The time series of meteorological parameters during the period of February 29 to March 5, 2016.

Figure S7. Time series of aerosol particle surface area in the absence and presence of aerosol particle liquid water (Left axis), as well as the ratio for a difference of surface area in the presence and absence of liquid water $((\text{Surface Area_wet} - \text{Surface Area_dry}) / \text{Surface Area_dry})$ (Right axis) during

60 February 29 to March 5, 2016.

Figure S8. Time series of aerosol particle volume in the absence and presence of aerosol particle liquid water (Left axis), as well as the ratio for difference of aerosol particle volume in the presence and absence of liquid water $((\text{Aerosol volume_wet} - \text{Aerosol volume_dry}) / \text{Aerosol volume_dry})$ (Right axis) during February 29 to March 5, 2016.

65 **Figure S9.** Time series of the ratio of the extinction coefficient for 300~700 nm and the total PM_1 in the presence of liquid water (Right axis) from February 29 to March 5, 2016.

Table S1. The classification of four modes of PNSD data (3 nm~10 μm) following results from long-term PNSD measurement in Beijing in Wu et al. (2008).

Text S1. Measurement and methods

75 *Size-resolved particle hygroscopicity (H-TDMA)*

Size-resolved hygroscopicity of sub-micrometer aerosol particles (50, 100, 150, 250, 350 nm) at 90% RH was measured by Hygroscopicity Tandem Differential Mobility Analyzer (H-TDMA, TROPOS, Germany). A detailed description of instrumentation and data quality control were shown in the Massling et al. (2011) and Wang et al. (2018). Here, only a brief introduction will be given. Mono-disperse aerosol particles were selected by the first Differential Mobility Analyzer (DMA, TROPOS, Germany). After humidification at 90% RH, particle number size distribution of humidified aerosol particles was measured by the second DMA coupled with a condensation particle counter (CPC, Model 3772, TSI, USA). Thus, the measurement density function (MDF) was obtained. The MDF was validated and inverted with TDMA_{inv} method (Gysel et al., 2009) to obtain particle's actual growth factor distribution (Growth Factor - Probability Density Function, GF-PDF). A series of Quality Assurance/Quality Control was adopted to ensure high-quality data. Ammonium sulfate aerosol particles were measured by H-TDMA every 4~5 hours during the campaign to ensure the stability and accuracy of RH in the system. The hygroscopicity of atmospheric aerosol particles in dry condition (RH<30%) was measured to validate the offset between measured HGF and 1 due to the different transfer functions of the two DMAs in the system. To eliminate the influences of RH fluctuation, all measured GF-PDFs in the condition of 87%<RH<93% were corrected to RH=90%. The equations of hygroscopic growth factor (*HGF*) and κ calculation are shown below:

The *HGF* of aerosol particles are defined as the particle mobility size at a given RH (D_{RH}) divided by the dry size (D_0):

$$HGF = \frac{D_{RH}}{D_0} \quad [S1]$$

The hygroscopicity parameter (κ) can be derived from HGF by κ -Köhler theory (Petters and Kreidenweis, 2007) in equation [S2-3].

$$\kappa = (HGF^3 - 1) \left(\frac{\exp\left(\frac{A}{D_0 \cdot HGF}\right)}{RH} - 1 \right) \quad [S2]$$

$$A = \frac{4\sigma_{s/a} M_w}{RT\rho_w} \quad [S3]$$

100 where HGF and D_0 represent the growth factor at 90% RH and dry size, respectively. $\sigma_{s/a}$ represents droplet surface tension (assumed to σ of the pure water, 0.0728 N/m^2), M_w and ρ_w are molecular weight and density of water respectively, R is the universal gas constant, and T is the absolute temperature. The obtained size-resolved hygroscopic parameter (κ) was used to calculate aerosol particle liquid water.

Size-resolved non-refractory chemical composition in PM₁ (HR-ToF-AMS)

A HR-ToF-AMS (High-Resolution Time-of-Flight Aerosol Mass Spectrometry, Aerodyne Research, Inc., USA) was applied to measure total mass concentration and size distribution of non-refractory chemical composition in PM₁, including ammonium (NH₄⁺), nitrate (NO₃⁻), sulfate (SO₄²⁻), 110 chloride (Cl⁻), and organic compounds. Detailed instrumentation was described previously in DeCarlo et al. (2006).

Only specific parameters and settings for the Instrument used will be given here. The AMS used for this study was modified by a quadrupole filter between the ionization region and the mass spectrometer. As fragmentation patterns of NH_4^+ , NO_3^- and SO_4^{2-} were found to be comparable to 115 standard AMS, it was shown that the quadrupole did not influence the transmission in the investigated m/z range (12~250 amu). Therefore, standard AMS data evaluation procedures were applied. Particle free air was used to determine detection limits for the AMS species throughout the whole campaign. The detection limit for organic (Org.), NH_4^+ , NO_3^- , SO_4^{2-} , and Cl^- mass concentrations were 0.424 $\mu\text{g}/\text{m}^3$, 0.005 $\mu\text{g}/\text{m}^3$, 0.029 $\mu\text{g}/\text{m}^3$, 0.011 $\mu\text{g}/\text{m}^3$, 0.023 $\mu\text{g}/\text{m}^3$, respectively.

120 Regular calibration was performed (approximately every 7~10 days; except during the 19 days of the Spring Festival break) using size-selected (350 nm) and dried NH_4NO_3 particles and a CPC (Model 3786, TSI, USA) as described in previous studies (Jayne et al., 2000; Jimenez et al., 2003). An average ionization efficiency (i.e. total response factor including the transfer efficiency of the ToF-MS) of $1.61 \pm 0.26 \times 10^{-8}$ was determined from all calibrations. This was subsequently used for the 125 determination of aerosol particle mass concentrations. Compound specific relative ionization efficiencies (RIE) for NH_4^+ and SO_4^{2-} were determined during following the standard calibration procedures. The RIE of Org, NH_4^+ , NO_3^- , SO_4^{2-} , Cl^- were 1.4, 2.71 ± 0.12 , 1.1, 1.54 ± 0.04 , 1.3, respectively.

130 A composition dependent correction factor was used to correct for non-unity collection efficiency (i.e. sampling of aerosol particles) (Middlebrook et al., 2012). Comparison of the retrieved AMS- PM_1 to PM_1 determined by an allocated Mobility Particle Size Spectrometer (MPSS) system showed that the total mass measured by the AMS on average accounted for 84 % and 73 % of the mass

measured by the MPSS assuming an effective aerosol particle density of 1.4 g/cm³ and 1.6 g/cm³, respectively. The density is expected to be within this range based the fact that the aerosol particle mass
135 consists of at least 50 % NH₄NO₃ and organics (both 1.4 g/cm³) and up to 50 % (NH₄)₂SO₄ (1.77 g/cm³) and NH₄HSO₄ (1.78 g/cm³). Taking into account that, (i) the AMS can only detect the non-refractory part of the aerosol particles and (ii) slight differences in the size ranges covered by AMS and MPSS, the agreement of PM₁ mass concentration measured by the two instruments is reasonable and assures that the AMS data can be quantitatively interpreted.

140 The AMS was located inside the building and air was sampling air through a 0.18' inner diameter (ID) stainless steel inlet line (2m length) that was further connected to a 0.255' ID stainless steel line coated with Silcoinert® (7.3m length). The total sampling flow through the inlet line was 1.82 L/min and the residence time of the air was approximately 10 s. Although the outside temperature was varying from -19.2 °C to 19.0 °C, the temperature at the AMS inlet was rather constant in the range of
145 20.0 °C to 26.5 °C. A Nafion drier (RH < 6 %) was applied upstream of the AMS and subsequently, the flow was split to a CPC (Model 3786, TSI, USA, flow rate: 0.60 L/min). In front of the Nafion drier, an optical particle counter (OPC, Model 1.129, Grimm, Germany) took a subsample of 1.16 L/min.

Positive matrix factorization (SoFi tool, ME2, Francesco Canonaco, PSI) was used to separate primary and secondary sources to the measured organic aerosol particle fraction. The factor indicating
150 primary organic sources from biomass burning (BBOA) could not be fully separated from other factors in a completely unconstrained PMF-run for the full data set. Therefore, the BBOA factor which was found in an unconstrained run of only the “clean period” was used to constrain it for the full dataset. The optimal solution to explain the current dataset was given by a 5-factor solution. This solution

contains 3 primary organic factors namely: biomass burning (BBOA), coal combustion (CCOA) and hydrocarbon like (HOA) as well as 2 oxygenated organic factors of one was more oxidized than the other factor (OOA1 - O/C ratio:0.32; OOA2 - O/C ratio: 0.48). OOA is frequently equated with secondary organic aerosol (SOA). Hence, the time series of mass concentration of primary organic aerosol (POA) and secondary organic aerosol (SOA) as well as the fraction of SOA in total organic was shown in Figure S1.

160

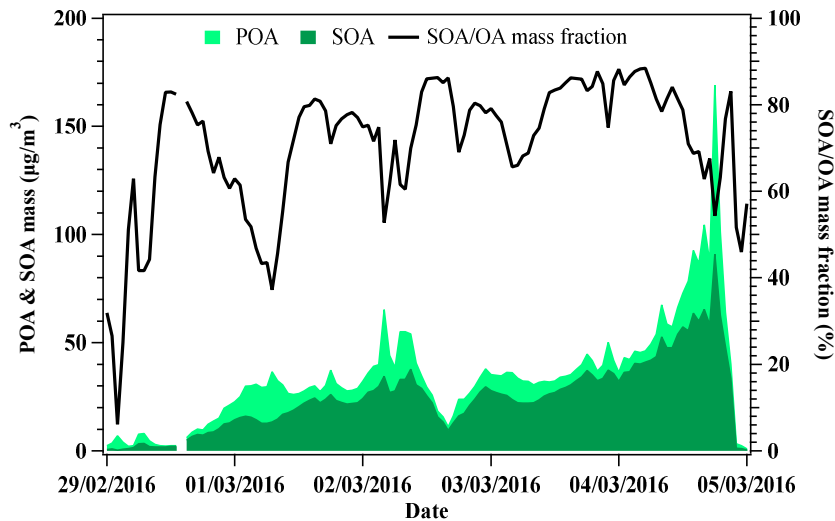


Figure S1. The time series of mass concentration of POA and SOA in non-refractory PM₁ from ME2 (left axis) and the fraction of SOA in total organic (right axis) during the period from 29 February to 5 March, 2016.

165

To calculate the size-resolved light extinction coefficient by Mie scattering model and $k_{\text{N}_2\text{O}_5}$, the liquid water and chemical composition of size-resolved particles need to be re-distributed as their size distributions were different and can't be combined directly. Therefore, the liquid water and chemical composition were re-distributed to the values of 100~200 nm, 200~300 nm, 300~400 nm, 170 400~500nm, 500~600 nm and 600~700 nm in stokes diameter. Here, the re-distribution method of AMS data was introduced below. Figure S2 showed one of the examples of the size distribution of $dM/d\log D_p$ in AMS data set. It is worth to note that particle size used in AMS was the aerodynamic diameter. Here, the optimized particle effective density of 1.5 g/cm³ was used to convert aerodynamic diameter to stokes diameter (Wu et al., 2016). That means the aerodynamic diameter of 150~300 nm, 175 300~450 nm, 450~600 nm, 600~750 nm, 750~900 nm, 900~1050 nm represents the stokes diameter of 100~200 nm, 200~300 nm, 300~400 nm, 400~500 nm, 500~600 nm, 600~700 nm respectively. As the $dM/d\log D_p$ is normalized, the $dM/d\log D_p$ of the particles in re-distribution size range was the sum of the $dM/d\log D_p$ of the covered particle size (as shown in Figure S2). For example, the $dM/d\log D_p$ for the 150~300 nm particles were the sum of $dM/d\log D_p$ of 100~102.54 nm, 102.54~117.24 nm, 180 117.24~134.05 nm, 134.05~153.26 nm, 153.26~175.23 nm, 175.23~200.36 nm, 200.36~229.08 nm, 229.08~299.47 nm, 199.47~300 nm. Finally, the sized-resolved chemical composition of 100~200 nm, 200~300 nm, 300~400 nm, 400~500 nm, 500~600 nm and 600~700 nm in stokes diameter were derived. The re-distribution method of liquid water to the values of 100~200 nm, 200~300 nm, 300~400 nm, 400~500nm, 500~600 nm and 600~700 nm in stokes diameter followed similar procedure as 185 described above and was not described repeatedly.

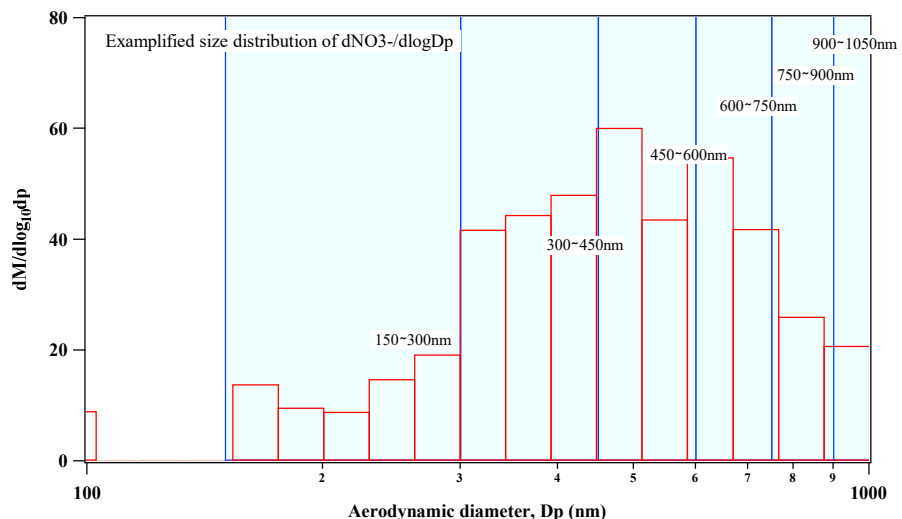
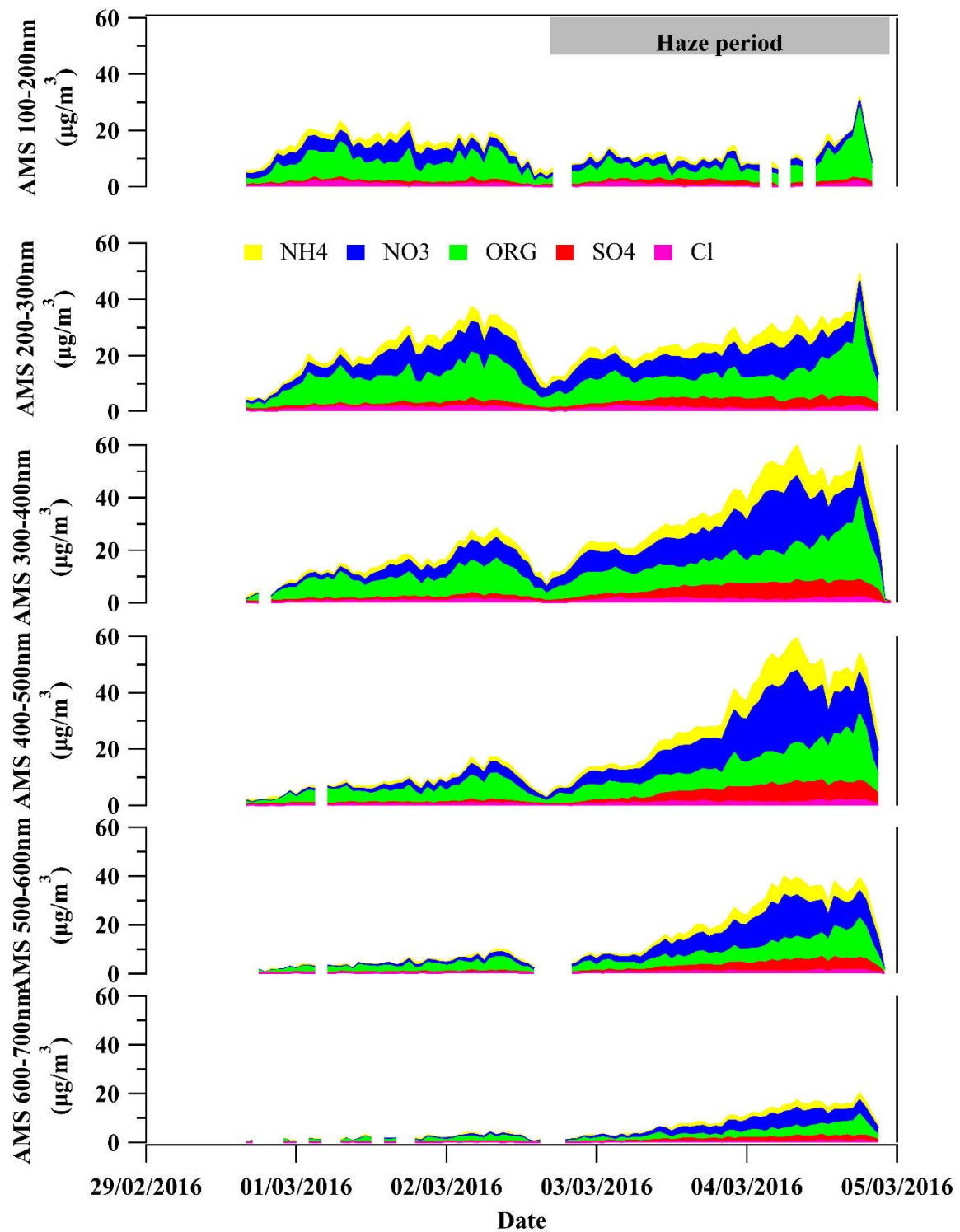


Figure S2. The exemplified size distribution of $dM/d\log D_p$ and the classification of re-arranged aerodynamic diameter size range.



190 **Figure S3.** Average size distribution of NH_4^+ , NO_3^- , SO_4^{2-} , Cl^- , Org (in stokes diameter), in the period of February 29 to March 5, 2016. During the marked heavily polluted episode, nitrate showed size distribution and nitrate in 300~700 nm particles (especially 400~600 nm) showed rapid enhancement with the development of haze event compared with constant sulfate mass concentration.

The measured mixing ratio of NH_3 and HNO_3 in the atmosphere (GAC-IC system)

195 GAC-IC system (Gas Aerosol Collector-Ion Chromatography) was performed to provide the water-soluble chemical composition in the gas phase (NH_3 , HCl , HONO , HNO_3 , SO_2) and aerosol particle phase (NH_4^+ , Na^+ , K^+ , Mg^{2+} , SO_4^{2-} , NO_3^- , Cl^-) with a time resolution of 30 mins. In this study, the measurement of gaseous HNO_3 was used to investigate the partitioning equilibrium between the gas and particle phase. A detailed description of the instrumentation of GAC-IC system can be found in

200 Dong et al. (2012). Briefly, ambient air was sampled by GAC-IC system. Sampling air was pumped through a wet denuder with coated absorption solution inside of denuder surface. Gaseous species were captured and collected by the wet denuder. Afterwards, particulate matter smaller than $2.5 \mu\text{m}$ was scavenged and collected by an aerosol collector. Finally, both gaseous and aerosol particle samples were measured by IC system (ICS-90, Dionex, USA) to provide chemical composition of water-soluble

205 species in gas and particle phase.

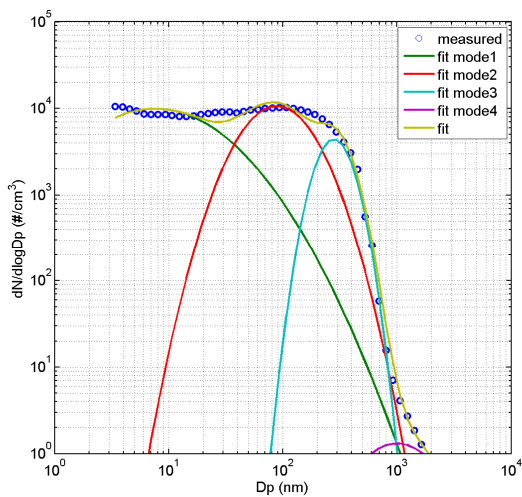
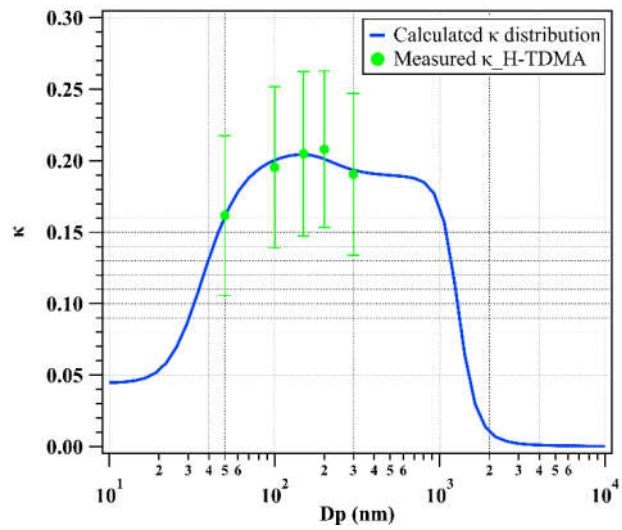


Figure S4. Comparison of particle number size distribution from measurement and four-mode lognormal fitting method.



215 **Figure S5.** Comparison of sized-resolved κ from H-TDMA measurement and the calculated size distribution of κ from 3 nm to 10 μm .

S2 Results

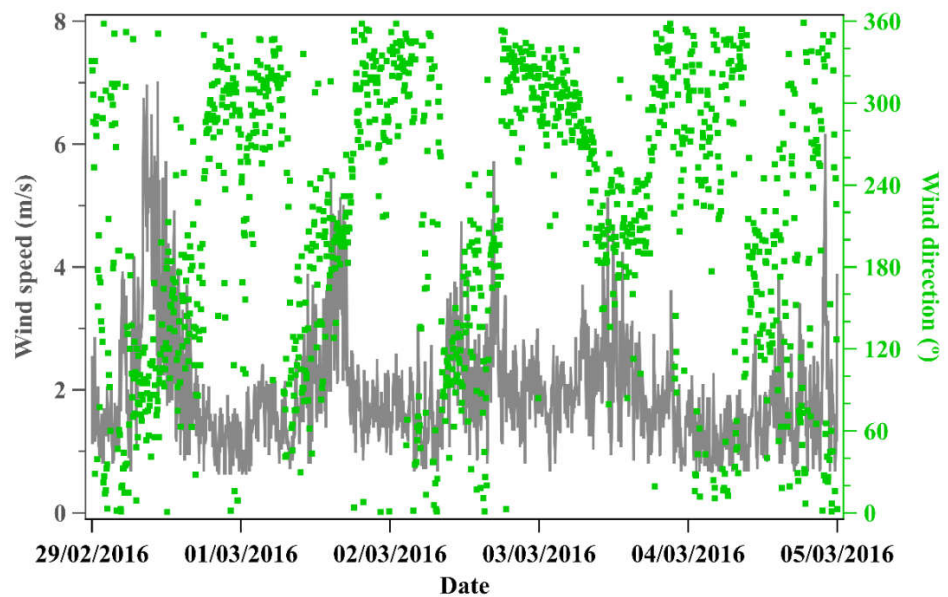


Figure S6. The time series of meteorological parameters during the period of February 29 to March 5,

220 2016.

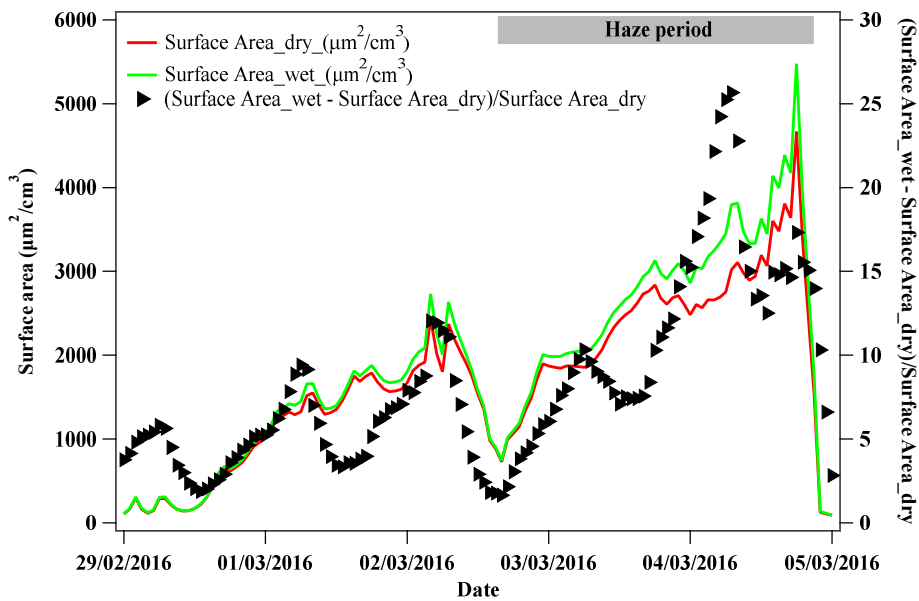
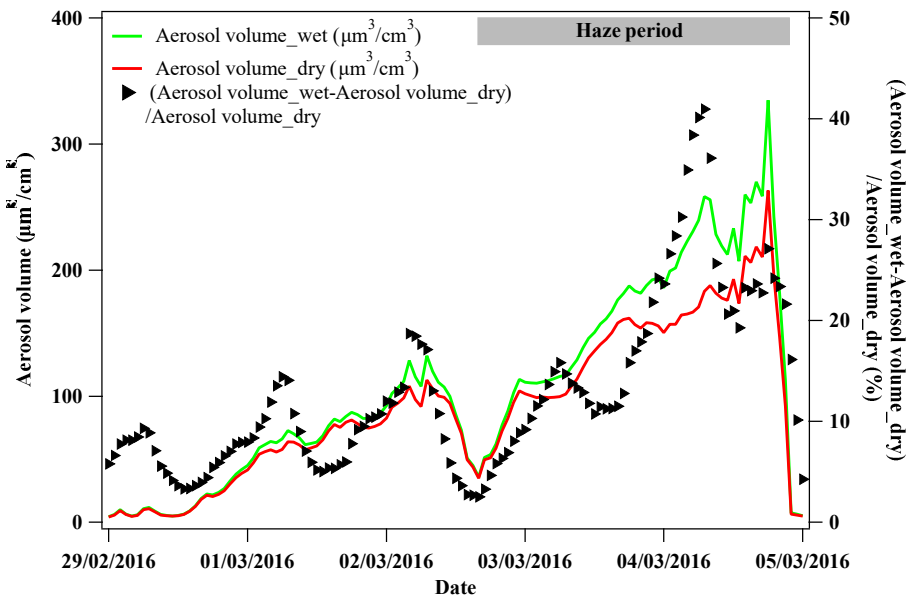


Figure S7. Time series of aerosol particle surface area in the absence and presence of aerosol particle liquid water (Left axis), as well as the ratio for a difference of surface area in the presence and absence 225 of liquid water $((\text{Surface Area}_\text{wet} - \text{Surface Area}_\text{dry})/\text{Surface Area}_\text{dry})$ (Right axis) during February 29 to March 5, 2016. The ratio of $(\text{Surface Area}_\text{wet} - \text{Surface Area}_\text{dry})/\text{Surface Area}_\text{dry}$ represents the aerosol particle surface area enhancement percentage due to the presence of liquid water compared to the dry condition.



230

Figure S8. Time series of aerosol particle volume in the absence and presence of aerosol particle liquid water (Left axis), as well as the ratio for difference of aerosol particle volume in the presence and absence of liquid water $((\text{Aerosol volume_wet} - \text{Aerosol volume_dry}) / \text{Aerosol volume_dry})$ (Right axis) during February 29 to March 5, 2016. The ratio of $(\text{Aerosol volume_wet} - \text{Aerosol volume_dry}) / \text{Aerosol volume_dry}$ represents the aerosol particle volume enhancement percentage due to the presence of liquid water compared to the dry condition.

235

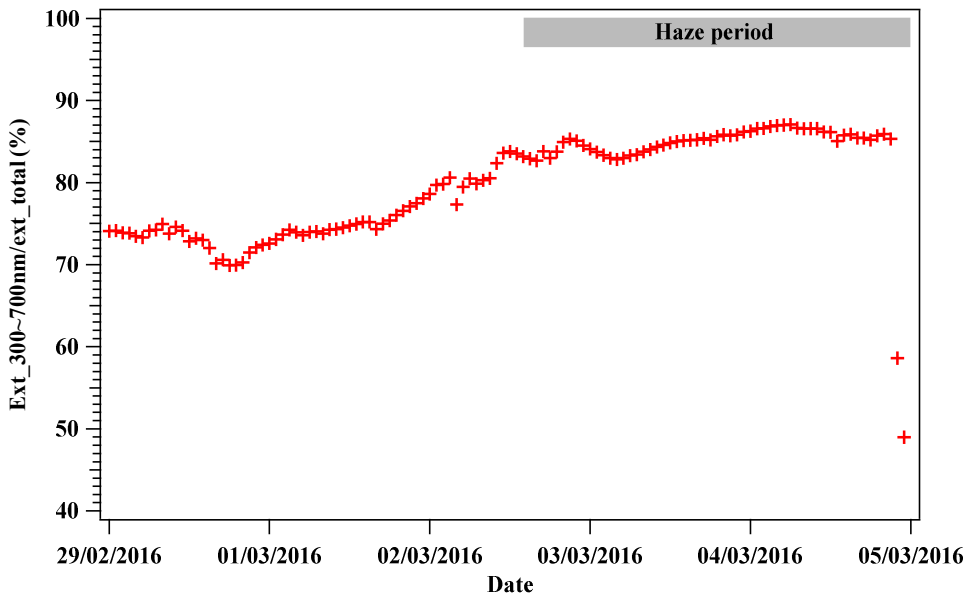


Figure S9. Time series of the ratio of the light extinction coefficient for 300~700 nm and the total PM_1 in the presence of liquid water (Right axis) from February 29 to March 5, 2016.

240

Table S1. The classification of four modes of PNSD data (3 nm~10 μm) following results from long-term PNSD measurement in Beijing in Wu et al. (2008). Particles from coarse mode were assumed hydrophobic with $\kappa_4 = 0$ following the method in Bian et al. (2014).

	Mode 1	Mode 2	Mode 3	Mode 4
Name	Nucleation mode	Aitken mode	Accumulation mode	Coarse mode
Size range	3-20 nm	20-100 nm	100 nm-1 μm	1 μm -10 μm
κ	κ_1	κ_2	κ_3	$\kappa_4 = 0$

245

References:

Bian, Y. X., Zhao, C. S., Ma, N., Chen, J., and Xu, W. Y.: A study of aerosol liquid water content based on hygroscopicity measurements at high relative humidity in the North China Plain, *Atmos. Chem. Phys.*, 14, 6417-6426, 10.5194/acp-14-6417-2014, 2014.

250 DeCarlo, P. F., Kimmel, J. R., Trimborn, A., Northway, M. J., Jayne, J. T., Aiken, A. C., Gonin, M., Fuhrer, K., Horvath, T., Docherty, K. S., Worsnop, D. R., and Jimenez, J. L.: Field-Deployable, High-Resolution, Time-of-Flight Aerosol Mass Spectrometer, *Analytical Chemistry*, 78, 8281-8289, 10.1021/ac061249n, 2006.

Dong, H. B., Zeng, L. M., Hu, M., Wu, Y. S., Zhang, Y. H., Slanina, J., Zheng, M., Wang, Z. F., and Jansen, R.: Technical Note: The application of an improved gas and aerosol collector for ambient air pollutants in China, 255 *Atmos. Chem. Phys.*, 12, 10519-10533, 10.5194/acp-12-10519-2012, 2012.

Gysel, M., McFiggans, G., and Coe, H.: Inversion of tandem differential mobility analyser (TDMA) measurements, 2, 134-151 pp., 2009.

Jayne, J. T., Leard, D. C., Zhang, X., Davidovits, P., Smith, K. A., Kolb, C. E., and Worsnop, D. R.: Development 260 of an Aerosol Mass Spectrometer for Size and Composition Analysis of Submicron Particles, *Aerosol Science and Technology*, 33, 49-70, 10.1080/027868200410840, 2000.

Jimenez, J. L., Jayne, J. T., Shi, Q., Kolb, C. E., Worsnop, D. R., Yourshaw, I., Seinfeld, J. H., Flagan, R. C., Zhang, X., Smith, K. A., Morris, J. W., and Davidovits, P.: Ambient aerosol sampling using the Aerodyne Aerosol Mass Spectrometer, *Journal of Geophysical Research: Atmospheres*, 108, doi:10.1029/2001JD001213, 2003.

Massling, A., Niedermeier, N., Hennig, T., Fors, E. O., Swietlicki, E., Ehn, M., Hämeri, K., Villani, P., Laj, P., 265 Good, N., McFiggans, G., and Wiedensohler, A.: Results and recommendations from an intercomparison of six Hygroscopicity-TDMA systems, *Atmos. Meas. Tech.*, 4, 485-497, 10.5194/amt-4-485-2011, 2011.

Middlebrook, A. M., Bahreini, R., Jimenez, J. L., and Canagaratna, M. R.: Evaluation of Composition-Dependent Collection Efficiencies for the Aerodyne Aerosol Mass Spectrometer using Field Data, *Aerosol Science and Technology*, 46, 258-271, 10.1080/02786826.2011.620041, 2012.

270 Petters, M. D., and Kreidenweis, S. M.: A single parameter representation of hygroscopic growth and cloud condensation nucleus activity, *Atmos. Chem. Phys.*, 7, 1961-1971, 10.5194/acp-7-1961-2007, 2007.

Seinfeld., J. H., and Pandis., S. N.: *Atmospheric Chemistry and Physics: from air pollution to climate change*, John wiley & Sons, INC, 2006.

275 Wang, Y., Wu, Z., Ma, N., Wu, Y., Zeng, L., Zhao, C., and Wiedensohler, A.: Statistical analysis and parameterization of the hygroscopic growth of the sub-micrometer urban background aerosol in Beijing, *Atmospheric Environment*, 175, 184-191, <https://doi.org/10.1016/j.atmosenv.2017.12.003>, 2018.

Wu, Z., Hu, M., Lin, P., Liu, S., Wehner, B., and Wiedensohler, A.: Particle number size distribution in the urban atmosphere of Beijing, China, 7967-7980 pp., 2008.

280 Wu, Z. J., Zheng, J., Shang, D. J., Du, Z. F., Wu, Y. S., Zeng, L. M., Wiedensohler, A., and Hu, M.: Particle hygroscopicity and its link to chemical composition in the urban atmosphere of Beijing, China, during summertime, *Atmos. Chem. Phys.*, 16, 1123-1138, 10.5194/acp-16-1123-2016, 2016.